



1 Causes for increased flood frequency in central Europe in the 19th century

2

3 Stefan Brönnimann,^{1,2,*} Luca Frigerio,^{1,2} Mikhaël Schwander,^{1,2,3} Marco Rohrer,^{1,2} Peter
4 Stucki,^{1,2} Jörg Franke^{1,2}

5

6 ¹ Oeschger Centre for Climate Change Research, University of Bern, Switzerland

7 ² Institute of Geography, University of Bern, Switzerland

8 ³ Federal Office of Meteorology and Climatology MeteoSwiss

9 * *correspondence to: stefan.broennimann@giub.unibe.ch*

10

11 Abstract

12 Historians and historical climatologists have long pointed to an increased flood frequency in Central Europe in
13 the mid and late 19th century. However, the causes have remained unclear. Here, we investigate the changes in
14 flood frequency in Switzerland based on long time series of discharge and lake levels, of precipitation and
15 weather types, and based on climate model simulations, focusing on the warm season. Annual series of peak
16 discharge or maximum lake level, in agreement with previous studies, display increased frequency of floods in
17 the mid 19th century and decreased frequency after the Second World War. Annual series of warm-season mean
18 precipitation and high percentiles of 3-day precipitation totals (partly) reflect these changes. A daily weather
19 type classification since 1763 is used to construct flood probability indices for the catchments of the Rhine in
20 Basel and the outflow of Lake Lugano, Ponte Tresa. The indices indicate an increased frequency of flood-prone
21 weather types in the mid 19th century and a decreased frequency in the post-war period, consistent with a climate
22 reconstruction that shows increased (decreased) cyclonic flow over Western Europe in the former (latter) period.
23 To assess the driving factors of the detected circulation changes, we analyse weather types and precipitation in a
24 large ensemble of climate model simulations forced with observed sea-surface temperatures. In the simulations,
25 we do not find an increase in flood-prone weather types in the Rhine catchment in the 19th century, but a
26 decrease in the post-war period related to the sea-surface temperature anomalies.

27

28 1. Introduction

29 Floods are some of the costliest natural hazards in Europe (EEA, 2018). In typical pluvio-
30 nival river regimes in Central Europe, floods are often triggered by one or several days of
31 heavy precipitation, but some rivers also exhibit winter floods due to longer periods of large-
32 scale precipitation or spring floods due to heavy precipitation, amplified by snow melt. Such
33 factors might change in the future. For instance, heavy precipitation events will become more



34 intense in the future according to global climate model simulations (Fischer and Knutti,
35 2016). An intensification of heavy precipitation events is also found in regional model
36 simulations for Europe north of the Mediterranean (Rajczak and Schär, 2017). With
37 increasing temperature, snow melt occurs earlier in the year, changing river regimes.
38 Furthermore, also precipitation extremes might shift seasonally (Brönnimann et al., 2018;
39 Marelle et al., 2018). While changes in seasonality have been found for European floods
40 (Blöschl et al., 2017), no general increase in flood frequency has so far been detected
41 (Madsen et al., 2014). However, past records suggest that there is considerable decadal
42 variation in flood frequency (e.g., Sturm et al., 2001; Wanner et al., 2004; Glaser et al., 2010).
43 It is reasonable to assume that such variations will continue into the future. In this paper we
44 focus on decadal variability during the past 200 years.

45 An increased flood frequency in the 19th century was already perceived by contemporary
46 scientists across central Europe and affected the political debates on deforestation as a
47 potential cause (e.g., Brückner, 1990). The changing frequencies of flood events in Central
48 Europe over the past centuries have been analysed in detail during the past 20 years (e.g.,
49 Mudelsee et al., 2004; Glaser et al., 2010). One result is that different river basins behave
50 differently due to different hydrological regimes and different seasonality of floods. For
51 instance, Glaser et al. (2010) found a prominent phase of increased flood frequency in central
52 European rivers from 1780 to 1840, but mainly in winter and spring. This may not apply to
53 Alpine rivers, which are more prone to floods in summer and autumn. Periods of increased
54 flood frequency have also been analysed with respect to reconstructions of atmospheric
55 circulation (e.g., Jacobeit et al., 2003; Mudelsee et al., 2004). Jacobeit et al. (2003) find that
56 the large-scale zonal mode, which characterizes flood events in the 20th century, does not
57 similarly characterize flood-rich periods during the Little Ice Age (their analysis, however,
58 does not cover the 19th century). For summer floods, Mudelsee et al. (2004) find a weak but
59 significant relation to meridional airflow. Quinn and Wilby (2013) were able to reconstruct
60 large-scale flood risk in Britain from a series of daily weather types back to 1871 and found
61 decadal scale change in circulation types.

62 For several catchments in the Alps and central Europe, studies have suggested an increased
63 frequency of flood events in the mid 19th century (Pfister 1984, 1999, 2009; Stucki and
64 Luterbacher, 2010; Schmocker-Fakel and Naef, 2010a,b; Wetter et al., 2011). However, the
65 causes of this increased flood frequency remain unclear. Besides human interventions such as
66 deforestation or undesigned effects from water flow regulations (Pfister and Brändli, 1999;
67 Summermatter, 2005), this includes the role of cold or warm periods and changes in



68 atmospheric circulation. Proxy-based studies, though focussing on longer time scales, find
69 that in the Alps, cold periods were mostly more flood prone than warm periods (Stewart et al.,
70 2011; Glur et al., 2013); the last of these cold and flood prone periods in the latter study is the
71 19th century. Glur et al. (2013) relate periods of increased flood frequency in the past 2500
72 years to periods of a weak and southward shifted Azores High. Even more remote factors
73 could have played a role. Using climate model simulations, Bichet et al. (2014) investigated
74 the roles of aerosols and of remote Pacific forcings on precipitation, albeit focusing on the
75 seasonal mean. Finally, Stucki et al. (2012) performed case studies of the strongest 24 flood
76 events of the last 160 years. They characterised five flood-conducting weather patterns,
77 although each extreme event had its individual combination of contributing factors.

78 In our paper, we aim to combine analyses of daily weather, reconstructions, and climate
79 model simulations to elucidate potential causes leading to an increased flood frequency in
80 Switzerland. While previous studies have focused on monthly or seasonal reconstructions, or
81 on individual cases, we study the daily weather back to the 18th century in a statistical
82 manner, thus bridging the gap between event analyses and paleo-climatological studies.

83 In this study we track the flood-frequency signal from historian documents to observations
84 and simulations. Using long data series on floods (discharge and lake level), precipitation,
85 daily weather types, and climate model simulations, we investigate whether an increased
86 frequency of flood events was due to a change in seasonal mean or extreme precipitation and
87 whether this can be related to change in weather conditions. We also address the underlying
88 hydro-meteorological and climatological causes in model simulations. The paper is organised
89 as follows. Section 2 describes the data and methods used. Section 3 describes the results. A
90 discussion is provided in Section 4. Conclusions are drawn in Section 5.

91

92 **2. Data and Methods**

93 *2.1. Discharge data*

94 For the analysis of the flood frequency, we used annual peak discharge measurements from
95 Basel, Switzerland, since 1808 (Wetter et al., 2011) as well as annual peak lake level data for
96 Lake Constance, Constance (since 1817, supplied by the German Landesanstalt für Umwelt,
97 Messungen und Naturschutz Baden-Württemberg) and Lago Maggiore, Locarno (Locarno
98 (Swiss Federal Office for the Environment FOEN) since 1868. The Lago Maggiore data were
99 corroborated by instrumental measurements at Sesto Calende for past floods since 1829 (Di
100 Bella, 2005) and by reconstructed lake levels for floods prior to that time both for Locarno



101 and Sesto Calende (Stucki and Luterbacher, 2010). Further, we used a daily discharge time
102 series for Basel and Ponte Tresa, Ticino, since 1901 from the FOEN. Figure 1 gives an
103 overview of the catchments and locations used in this paper.

104 Some of the series have potential inhomogeneities. Major corrections in the catchments or
105 lakes were carried out in 1877 (Jura Waters correction, affecting the Aare and thus the Rhine),
106 between 1888 and 1912 (Ticino in the Magadino plain), and 1943 (regulation of the level of
107 Lago Maggiore). Lake Constance was and still is unregulated, but Jöhnk et al. (2004) argue
108 that the level decreased by 15 cm between 1940 and 1999 due to upstream reservoirs. Based
109 on model simulations, Wetter et al. (2011) estimate that the Jura Waters correction led to a
110 reduction of peak discharges in Basel by 500 to 630 m³/s. A further possible inhomogeneity
111 concerns the level of Lago Maggiore. The flood of 1868 reportedly has led to erosion at the
112 outflow, lowering the peak lake levels after the event. We will address these issues in Sect. 3.

113

114 *2.2. Precipitation data*

115 Unfortunately, hardly any daily precipitation series covers the entire, approx. 200- year period
116 considered here. The only long series in Switzerland is from Geneva (Fülleemann et al., 2011),
117 with daily precipitation data reaching back to 1796. Note that this series has not been
118 homogenized prior to 1864, and that it might not be representative for the northern side of the
119 Alps. Much more daily records exist from Switzerland from 1864 onward, the start of the
120 Swiss network. We use data for Lugano (Ponte Tresa catchment), as well as from a number of
121 other stations (Affoltern, Basel, Altstätten, Bellinzona, Lohn, Engelberg, see Fig. 1). Monthly
122 precipitation was taken from the gridded HISTALP data set (Hiebl et al., 2009).

123 Earlier studies (e.g., Glaser et al., 2010; Stucki et al., 2012) indicate that in the region of
124 interest, most floods occur in the warm season (hereafter May to October). The only notable
125 exception is the Christmas flood of 1882. In this paper, we therefore show the results only for
126 the warm season. From both daily precipitation series we calculate the maximum precipitation
127 amount over 3 days per warm season, denoted Rx3day. From the gridded HISTALP data set
128 we calculated warm season precipitation averages for two regions (Fig. 1): A region north
129 [46.5-47.5°N, 6.5-10°E] and a region south [45.75-46.25°N, 8.5-9.25°E] of the Alpine divide.

130

131 *2.3. Weather type reconstruction*

132 In order to address flood-inducing weather patterns, we use the daily weather type
133 reconstruction for Switzerland by Schwander et al. (2017), which reaches as far back as 1763.



134 The weather types used in this paper are an extension of the CAP9 weather types of
135 MeteoSwiss (Weusthoff, 2011) into the past, using station data and classifying each day
136 according to its Mahalanobis distance from the centroids of the weather types in the
137 calibration period. However, as two of the types were not well discernible from two other
138 types, the respective types were merged such that only seven types remain (CAP7, see
139 Schwander et al., 2017).

140

141 *2.4. Climate model simulations and reconstructions*

142 For the analysis of atmospheric circulation during the 19th and 20th century, we use the
143 reconstruction EKF400 (Reconstruction by Ensemble Kalman Fitting over 400 years, Franke
144 et al., 2017). This global, three-dimensional reconstruction is based on an off-line data
145 assimilation approach of early instrumental, documentary and proxy data into an ensemble of
146 climate model simulations. It provides an ensemble of 30 monthly reconstructions back to
147 1600. Here we use the ensemble mean and analyse geopotential height (GPH) and vertical
148 velocity at 500 hPa, wind at 850 hPa as well as precipitation.

149 Finally, we compare the observations-based results with a large ensemble of climate model
150 simulations. We use a 30-member ensemble of atmospheric simulations performed with
151 ECHAM5.4 (T63) termed CCC400 (Chemical Climate Change over 400 years), which is the
152 set of simulations that also underlies EKF400. The simulations cover the period 1600 to 2005
153 and are described in Bhend et al. (2012). Their most important boundary conditions are sea-
154 surface temperature (SST) data by Mann et al. (2009). From these SSTs we also calculated
155 indices of the Atlantic Multidecadal Oscillation (AMO) and the Pacific Decadal Oscillation
156 (PDO) following the definitions by Trenberth and Shea (2006) and Mantua et al. (1997),
157 respectively (see Brönnimann, 2015, for extensive comparisons of these indices and CCC400
158 results). Note that in these simulations, the long-term changes in land-surface properties were
159 misspecified. We therefore performed an additional simulation with corrected land surface to
160 assess the impacts (Rohrer et al., 2018). While no impacts were found in heavy precipitation
161 and weather types, warm-season average precipitation showed a too strong drying trend,
162 which we adjusted to match that of the corrected simulation. In any case, the discrepancy
163 concerns the long-term change and not decadal-to-multidecadal variability.

164 For the analysis in this paper, we use daily precipitation representative of the Aare catchment
165 (47.5° N/7.4° E, see Brönnimann et al., 2018) and the CAP7 weather types from CCC400.

166 The CAP7 weather types were evaluated by Rohrer et al. (2018): Although the model shows a



167 zonal bias (too frequent westerly types), the decadal variability of weather type frequencies
168 within the simulations may give some indications as to possible contribution forced by SST
169 anomalies or other forcings.

170

171 2.5. Construction of a flood probability index

172 From the weather types described above, we construct a flood probability index (FPI) for each
173 river catchment following the basic methodology of Quinn and Wilby (2013). The FPI weighs
174 the frequency of weather types according to their flood-proneness. To determine the weights,
175 we used daily discharge data during the period 1901-2009 for Basel and Ponte Tresa. Flood
176 events were defined using a peak-over-threshold approach. The 98th percentile of warm
177 season days was taken as a threshold, and a declustering was applied by combining events
178 with a maximum distance of 3 days. Compositing the events around the day of maximum
179 discharge showed enhanced discharge already 2-4 days prior to the event. Therefore, we also
180 considered weather types on the three days prior to the event, consistent with results by
181 Froidevaux (2014) on the role of antecedent precipitation for floods in Swiss rivers.

182 A seasonal or annual flood probability index FPI_y can be defined in the following way. For all
183 event days (and similarly for preceding days, l indicates the lag and ranges from -3 to 0), we
184 analysed the frequency of a given weather type t relative to all event days and divided this by
185 the overall frequency of that weather type on all days. This ratio was termed w_{tl} :

$$186 \quad w_{tl} = \frac{n_{tl}/n_l}{n_t} \quad (1)$$

187 To determine the FPI for a given year y (in our case, a warm season) we analysed the absolute
188 weather type frequencies in that year (warm season), f_{ty} , and multiplied it with the
189 corresponding weights w_{tl} for a given lag l . This results in one time series for each lag l . The
190 four series were then combined to provide the index FPI_y using a weighted average with
191 weights v_l :

$$192 \quad FPI_y = \sum_l v_l \sum_t f_{ty} w_{tl} \quad (2)$$

193 We tested two sets of weights (v_l) for days -3 to 0: a ramp function (1/9, 2/9, 3/9 and 3/9), or
194 equal weight (0.25, 0.25, 0.25, 0.25). Correlations of the resulting indices were very high
195 (0.995 and 0.988 for Basel and Ponte Tresa, respectively) and only the former results are
196 shown in the following.



197 Figure 2 (top) shows the frequency of weather types during the warm season for the period
 198 1901-2000. The types „northeast, indifferent“ and „west-southwest, cyclonic“, and „east,
 199 indifferent“ make up 60% of all days. The most rare weather type „high pressure“ accounts
 200 for 5% of all days. The middle and bottom panels show the fraction of flood events per
 201 weather type for Basel and Ponte Tresa (dividing the fractions in the bottom panels series by
 202 the frequencies in the top panel yields w_{it}). Of all flood days in Basel, 60% are either
 203 „northeast indifferent“ or „north cyclonic“ types. Results are similar for the days before; 44%
 204 of these are of the „north cyclonic“ type, which is 3.4 times more frequent than over all days
 205 (top). With increasing lead time, „west-southwest cyclonic“ days become more prominent.
 206 For Ponte Tresa, type 7 („westerly over southern Europe, cyclonic“) is the most flood prone,
 207 while „west-southwest cyclonic“ dominates on the preceding days. The enhancement of flood
 208 probability is largest for type 7 the day before the event (floods are 4.8 times more frequent).

209 Quinn and Wilby (2013) used annual frequencies of the weather types to define the FPI. Here
 210 we calculated a daily index FPI_d , which (unlike the annual index) takes the actual sequence of
 211 weather types into account, such as during the passage of a cyclone. Equation (2) can be used
 212 for the daily index, with the same weights v_l and w_{it} as for FPI_y , but the frequency f_{idl} is now
 213 either zero or one:

$$214 \quad FPI_d = \sum_l v_l \sum_t f_{idl} w_{it} \quad (3)$$

215 The result is a daily index FPI_d whose warm season average is by definition equal to FPI_y , but
 216 which allows also studying other statistics. To test the daily index, we studied composites of
 217 FPI_d for Basel for all peak-over-threshold flood events and conversely composites of
 218 discharge for peak-over-threshold events of FPI_d (defined in the same way, i.e., as declustered
 219 98th percentile). As expected, flood events are related to a clearly increased FPI_d (Fig. 3, top).
 220 The average reaches 1.73, which means a 73% increase in flood probability. This corresponds
 221 roughly to the 80th percentile of FPI_d . Compositing discharge for instances with a high FPI_d
 222 (Fig. 3, bottom) shows increased discharge near its 70th percentile. Thus, the index captures
 223 flood events well, although with a high rate of „false alarms“ (i.e., not all FPI_d events lead to
 224 floods). This can be expected for such a coarse classification (only 7 types). Not every
 225 passage of a cyclone leads to a flood, and „optimal“ flood-inducing 4-day sequences of
 226 weather types are reached rather frequently. Based on these results, we chose the annual warm
 227 season 50th and 75th percentile of FPI_d for the following analyses, together with FPI_y (i.e., the
 228 mean of FPI_d).

229



230 **3. Results**

231 *3.1. Flood frequency*

232 To begin with, we analysed the flood series in order to test whether the reported increased
233 flood frequency in the mid-19th century is also found in our series (Fig. 4). The first thing we
234 note is that floods do not occur synchronously across the considered catchments. The same is
235 true for annual peak discharge series in general, as evidenced by low Spearman correlations.
236 For instance, the series for the Rhine in Basel is uncorrelated with the series of Lago
237 Maggiore and only moderately (coefficient of 0.36) with the series of Lake Constance, even
238 though the latter comprises a large sub-catchment.

239 Was flood frequency higher in the mid-19th century? In fact, each series exhibits prominent
240 peaks in the 19th century, e.g., the Rhine in Basel in 1817, 1852, 1876, 1881, and 1882 (see
241 Stucki et al., 2012), Lake Constance in 1817 (see Rössler and Brönnimann, 2018) and Lago
242 Maggiore in 1868. However, we also note a period of low flood frequency in Basel from the
243 1920s to 1970s, in agreement with a low frequency of peak-over-threshold events in Basel
244 and Ponte Tresa. For further analyses we defined the 30 yr periods with highest and lowest
245 flood frequencies, respectively, as follows: From the annual series we defined floods as
246 exceedances of the 95th percentile of the 1901-2000 period (dashed line). Note that even
247 accounting for a shift of 630 m³/s due to the Jura Waters correction would not change the
248 selected events of the Rhine in Basel, neither would a correction for a linear 15 cm trend of
249 Lake Constance after 1940 due to an increasing number of water reservoirs upstream (cf.
250 Jöhnk et al., 2004). However, the inhomogeneity caused by the 1868 event might be
251 substantial. We therefore considered pre-1968 data only qualitatively.

252 Counting annual floods in all series as well as counting the daily peak-over-threshold events
253 for Basel and Ponte Tresa both yields the same 30-yr period with lowest flood frequency:
254 1943-1972. The period with highest flood frequency is only defined by counting annual
255 floods. Not including pre-1868 Lago Maggiore data, the period 1847-1876 is the most flood-
256 rich. This is further supported by the historical data for Lago Maggiore, which suggest
257 additional strong flood events in that period. However, earlier 30-yr periods might be equally
258 or even more flood-rich, according to reconstructed flood events.

259 In the following we assess differences in a variable in each period relative to a corresponding
260 climatology (a sample consisting of 30 yrs before and 30 yrs after the period to further reduce
261 the effect of centennial-scale changes) as well as between the two periods with a Wilcoxon
262 test.



263

264 3.2. Precipitation

265 In a second step, we analysed warm-season mean precipitation and Rx3day for the regions
266 north or south of the Alps (Figs. 5 and 6). In both regions, warm season precipitation is
267 correlated significantly (Spearman correlation of 0.45 and 0.50, respectively) with annual
268 maximum discharge, clearly indicating that the floods under study are caused by excess
269 precipitation. In both regions, precipitation was slightly above the 20th century mean (dashed)
270 during most of the 19th century and below average during the flood-poor period. The
271 difference between the flood-rich and the flood-poor periods is significant ($p = 0.027$) for the
272 Ponte Tresa catchment. For the Basel catchment, both periods deviate significantly negatively
273 from the corresponding neighbouring decades ($p = 0.049$ and 0.030 for the flood-rich and
274 flood-poor period, respectively), which is unexpected for the flood-rich period. Their
275 difference is not significant.

276 Rx3day for Geneva and Lugano are shown exemplarily to assess the role of extreme
277 precipitation. For Geneva, we find two pronounced extremes (1827, 1888), both of which
278 were discussed in newspapers (e.g., Biliothèque universelle, **35**, 53) and thus are considered
279 real. For both stations, the decreased intensity of Rx3d in the flood-poor period relative to
280 neighbouring decades is significant ($p = 0.026$ and 0.038 for the Rhine and Ponte Tresa
281 catchments, respectively). A similar decrease at the same time is also found for other series in
282 Switzerland (Fig. 7 shows 6 long series). Calculating for each series the annual exceedance
283 frequency of the 95th percentile (based on the 1901-2000 interval) of Rx3d and then averaging
284 over all 8 series shown in Fig. 5 to 7, we obtain a time series of the ratio of stations exceeding
285 their 95th percentile in a given year. This series shows lower values in the 1943-1972 period
286 than in the following 30 year period and even lower than in the late 19th century.

287 In Section 3.1 we found clear changes in flood frequency. This section shows that at least the
288 flood-poor period was related to a reduction in the precipitation amount and intensity of Rx3d
289 events, while results for the flood-rich period are ambiguous.

290

291 3.3. Weather and large-scale flow

292 In a third step, we analyse the link of flood events to atmospheric circulation and its
293 multidecadal changes by means of the FPI_d statistics (see Sect. 2.5). The temporal
294 development for Basel (Fig. 5, bottom) and Ponte Tresa (Fig. 6, bottom) is similar for all
295 indicators (mean, median or 75th percentile), and the Spearman correlations of the Basel FPI_d



296 series with the annual maximum discharge at Basel are statistically significant ($p = 0.003$ to
297 0.004). This shows that the FPI is a good predictor for flood variability.

298 For both catchments, the indices reveal clear multidecadal variability. Indices are generally
299 positive from the 1810s to 1900s (with a secondary maximum in the 1920s and 1930s) and
300 negative from the 1940s to around the 2000s. Both periods are longer than those selected in
301 our study. The differences in the FPI_d between our flood-rich and flood-poor period is
302 significant in both catchments for all three indices (max. p-value is 0.0022). The flood-rich
303 period does not differ significantly from the neighbouring decades (which also show high
304 values of the FPI) in any of the indices, whereas the flood-poor period shows lower values
305 than the neighbouring decades ($p = 0.089$ and 0.008 for Basel and Ponte Tresa, respectively).
306 From these analyses we can conclude that the change in precipitation amount and intensity
307 found in the previous Section was related to the FPI . The flood-rich and flood-poor periods
308 clearly differ with respect to occurrence of weather types, i.e. large-scale atmospheric flow.

309 To further assess these differences in the large-scale atmospheric patterns, we also analysed
310 the two periods in global climate reconstructions (EKF400), each relative to its climatology as
311 well as the difference between the two (Fig. 8). The anomalies for the flood-rich period show
312 clear negative GPH anomalies over western Europe and strengthened flow from the north-
313 west. The extension of the Azores onto the European continent weakened. This pattern
314 becomes a lot stronger and clearer when contrasting the two periods (flood-rich minus food-
315 poor). The anomalies for the flood-poor period show strengthened high-pressure influence
316 over Central Europe, descent, and dryness with anomalous flow from the north east.

317 In all, the large-scale analysis confirms the results from the FPI : It shows clearly that the shift
318 in weather types was an expression of multi-decadal variability of atmospheric circulation
319 over the full North Atlantic-European sector, consisting of a more zonal and southward-
320 shifted circulation.

321

322 3.4. Climate model simulations

323 We have seen that the decadal-to-multidecadal changes in flood frequency can be related to
324 changes in weather types, which are part of large-scale flow anomalies. In the fourth step, we
325 analysed whether this can in turn be attributed to forcings as depicted in atmospheric model
326 simulations, i.e. in the CCC400 model. Concretely, we analysed warm-season mean
327 precipitation and Rx3d for a grid point north of the Alps and calculated FPI_d and its statistics
328 for each member. We then averaged the results across all 30 CCC400 members. As the signal-



329 to-noise ratio is small and year-to-year fidelity might be misleading, Figure 9 shows the series
330 in a smoothed form (31-yr moving average) for visualisation.

331 Indeed, we note that the agreement between modelled and observation-based FPI is not good
332 in the 19th century; the broad 19th century peak in the observation-based FPI is missing in the
333 model. In addition, the analysis reveals downward trends in mean precipitation (although the
334 series is trend-corrected) as well as in Rx3d. Quantitatively, the trend in mean precipitation
335 amounts to -1.88% per century, which is rather small (much smaller than in the observations).
336 Due to this trend it is not surprising that significant differences in seasonal mean precipitation
337 between the two periods appear. Irrespective of obvious deficiencies in the model, however, a
338 significant difference also appears for FPI_y between the two specified periods ($p = 0.005$),
339 showing that there is forced multidecadal variability in the model.

340 In the model, the flood-rich period is not significantly different from neighbouring decades in
341 any of the measures, but the flood-poor period clearly appears as a potentially flood-poor
342 period, both in seasonal mean precipitation ($p = 0.006$) and FPI_y . ($p = 0.038$). Only model
343 boundary conditions can explain this, and the arguably dominant contribution is from SSTs.
344 Among the well-known SST variability modes, it is in fact the PDO index that explains the
345 FPI_y most successfully. However, the Spearman correlation (0.138) remains low and not
346 significant in view of the low number of degrees of freedom, even after detrending.

347 We infer from these analyses that our climate model simulations partly reproduce the
348 sequence of flood-rich and flood-poor periods. However, the amplitude of the signal is very
349 small and only the flood-poor period appears as a significant feature, possibly forced by
350 changing sea-surface temperature in the North Pacific.

351

352 4. Discussion

353 While tracking the flood-frequency signal, we have found a number of links and
354 dependencies; these are discussed in the following. For instance, previous studies found an
355 increased flood frequency in Switzerland in the 19th century (Pfister 1984, 1999, 2009; Stucki
356 and Luterbacher, 2010; Schmocker-Fackel and Naef, 2010a,b; Wetter et al., 2011) as well as a
357 decrease in the mid 20th century, sometimes referred to as the „disaster gap“ (Pfister, 2009;
358 Wetter et al., 2011). The series used in this paper confirm the general tendency. Schmocker-
359 Fackel and Naef (2010a,b) identify 1820-1940 as a flood-rich period, while we use much a
360 shorter period. However, our FPI is consistent with a longer flood-rich period around 1820-



361 1940, i.e., the difference between 1820-1940 and 1943-1972 is also highly significant ($p <$
362 0.00001).

363 Warm season mean precipitation shows changes that are concurrent with those of flood
364 frequency, with significant correlations. Rx3day series from Geneva and Lugano together
365 with series from a larger number of Swiss stations confirm a multidecadal period around the
366 1960s with reduced intensity of Rx3d.

367 Schmocker-Fackel and Näf (2010a) analysed the relation between floods and weather types
368 for the period after 1945 and manual assignments based on weather reports before that year.
369 Here we can make use of a new, daily 250-yr weather type reconstruction. As in Schmocker-
370 Fackel and Näf (2010a), we find that events south of the Alps and those north of the Alps are
371 related to slightly different weather type characteristics, although indices for both regions are
372 highly correlated on all time scales. Our *FPI* shows clear multidecadal variability, with high
373 values during most of the 19th century and a secondary peak in the 1920s and 1930s, and
374 lower than average values in the post-war period. After around 1980, the FPI returned to
375 average values.

376 In agreement with Schmocker-Fackel and Näf (2010a,b), we find no imprint on the classical
377 NAO pattern and also no clear weakening of the Azores high during the flood-rich period.
378 However, we find that the extension of the Azores onto the European continent weakened,
379 and we find clear negative GPH anomalies over western Europe, strengthened north-westerly
380 advection, and large-scale ascent. This indicates a more zonal, southward-shifted circulation
381 over the North Atlantic-European sector during the flood-rich period. Opposite anomalies,
382 i.e., positive GPH anomalies and descent, are found for the flood-poor period, which was in
383 fact associated with heatwaves and strong droughts in Central Europe. Brugnara and Maugeri
384 (2019), find a regime shift in total precipitation and wet-day frequency for a southern region
385 of the Alps, and for a period after the 1940s which coincides with the flood-poor period.

386 The flood-poor period might carry imprints of oceanic forcing. Sutton and Hodson (2005)
387 related summer climate anomalies on both sides of the Atlantic in the wider 1931-1960 period
388 to changes in the AMO. We do not find a significant correlation between our flood and
389 precipitation indicators and the AMO, but a possible relation to the PDO index that needs to
390 be further explored. The flood-poor period partly overlaps with a period of poleward
391 displacement of the northern tropical belt, which is understood to be caused by sea-surface
392 temperature anomalies and is reproduced in climate models (Brönnimann et al., 2015). Our
393 EKF400 analysis is thus consistent with the results of the latter study.

394 **5. Conclusions**

395 Flood frequency in Central Europe exhibits multidecadal changes, which has been
396 demonstrated based on historical records. The causes for the increased flood frequency in
397 Switzerland in the 19th century as well as for the decreased flood frequency around the mid-
398 20th century are long-standing issues. In this study we have tracked these changes from flood
399 records through precipitation records, weather type statistics and large-scale circulation
400 reconstructions all the way to oceanic forcing as expressed in climate model simulations. Here
401 we attribute the changes in flood frequency to changes in mean precipitation and in the
402 intensity of Rx3d. In turn, these are related to a change in cyclonic weather types over Central
403 Europe. These changes indicate a shift in large-scale atmospheric circulation, with a more
404 zonal, southward shifted circulation during the flood-rich period relative to the flood poor
405 period. Precipitation and circulation changes are also partly reproduced in climate model
406 simulations forced by sea-surface temperature. However, only a very small part of the signal
407 is recovered, which points to random atmospheric variability as an important cause.

408 The analyses show that decadal variability in flood frequency occurred in the past; and is
409 likely to continue into the future. Better understanding its relation to weather regimes, large-
410 scale circulation, and possibly sea-surface temperature may help to better assess seasonal
411 forecasts and projections. Finally, the study also shows that the Quinn and Wilby (2013)
412 methodology also works for flood risk in Switzerland.

413

414 *Acknowledgements:* This work was supported by Swiss National Science Foundation projects
415 RE-USE (162668), EXTRA-LARGE (143219), and CHIMES (169676), by the European
416 Commission (ERC Grant PALAEO-RA, 787574) and by the Oeschger Centre for Climate
417 Change Research. Simulations were performed at the Swiss National Supercomputing Centre
418 CSCS.

419

420 **References**

- 421 Bhend, J., Franke, J., Folini, D., Wild, M., and Brönnimann, S.: An ensemble-based approach to
422 climate reconstructions, *Clim Past* 8, 963–976, 2012.
- 423 Bichet, A., Folini, D., Wild, M., and Schär, C.: Enhanced Central European summer precipitation in
424 the late 19th century: a link to the Tropics, *Q. J. Roy. Meteorol. Soc.*, 140, 111–123, 2014.
- 425 Blöschl, G. et al.: Changing climate shifts timing of European floods, *Science*, 357, 588–590, 2017.
- 426 Brönnimann, S.: Climatic changes since 1700. Springer, *Advances in Global Change Research Vol.*
427 55, xv + 360 pp., 2015.
- 428 Brönnimann, S., Fischer, A. M., Rozanov, E., Poli, P., Compo, G. P., Sardeshmukh, P. D.: Southward
429 shift of the Northern tropical belt from 1945 to 1980, *Nat. Geosci.*, 8, 969–974, 2015.



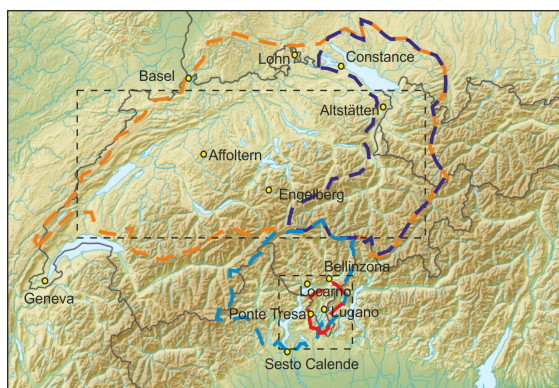
- 430 Brönnimann, S., Rajczak, J., Fischer, E., Raible, C. C., Rohrer, M., and Schär, C.: Changing
431 seasonality of moderate and extreme precipitation events in the Alps, *Nat. Haz. Earth Sys. Sci.*, 18,
432 2047–2056, 2018.
- 433 Brückner, E.: *Klimaschwankungen seit 1700 nebst Bemerkungen über die Klimaschwankungen der*
434 *Diluvialzeit*. E. D. Hölzel, Wien and Olmütz, 1890.
- 435 Brugnara, Y., and Maugeri, M.: Daily precipitation variability in the southern Alps since the late 19th
436 century (submitted), 2019.
- 437 Di Bella, G.: *Le Piene del Ticino a Sesto Calende*, Cocquio Trevisago, available at:
438 <http://www.prosestocalende.it/> (last access: 21 January 2019), 2005.
- 439 EEA: *Economic losses from climate-related extremes*. Copenhagen, Denmark, 17 pp., 2018.
- 440 Fischer, E. M., and Knutti, R.: Observed heavy precipitation increase confirms theory and early
441 models, *Nat. Clim. Ch.*, 6, 986–991, 2016.
- 442 Froidevaux, P.: *Meteorological characterisation of floods in Switzerland*. PhD Thesis, University of
443 Bern, 2014.
- 444 Fülleemann, C., Begert, M., Croci-Maspoli, M., and Brönnimann, S.: Digitalisieren und
445 Homogenisieren von historischen Klimadaten des Swiss NBCN – Resultate aus DigiHom,
446 *Arbeitsberichte der MeteoSchweiz*, 236, 48 pp., 2011.
- 447 Glaser, R. et al.: The variability of European floods since AD 1500, *Climatic Change*, 101, 235–256,
448 2010.
- 449 Glur, L., Wirth, S. B., Büntgen, U., Gilli, A., Haug, G. H., Schär, C., Beer, J., and Anselmetti, F. S.:
450 Frequent floods in the European Alps coincide with cooler periods of the past 2500 years, *Sci.*
451 *Rep.*, 3, 2770, 2013.
- 452 Hiebl, J., Auer, I., Böhm, R., Schöner, W., Maugeri, M., Lentini, G., Spinoni, J., Brunett, M., Nanni,
453 T., Tadic, M. P., Bihari, Z., Dolinar, M., and Müller-Westermeier, G.: A high-resolution 1961–1990
454 monthly temperature climatology for the greater Alpine region, *Meteorol. Z.*, 18, 507–530, 2009.
- 455 Jacobeit, J., Glaser, R., Luterbacher, J., and Wanner, H.: Links between flood events in Central Europe
456 since AD 1500 and large-scale atmospheric circulation modes, *Geophys. Res. Lett.*, 30, 1172–1175,
457 2003.
- 458 Jöhnk, K. D., Straile, D., and Ostendorf, W.: Water level variability and trends in Lake Constance in
459 the light of the 1999 centennial flood, *Limnologica* 34, 15–21, 2004.
- 460 Madsen, H., Lawrence, D., Lang, M., Martinkova, M., and Kjeldsen, T. R.: Review of trend analysis
461 and climate change projections of extreme precipitation and floods in Europe, *J. Hydrol.*, 519,
462 3634–3650, 2014.
- 463 Mann, M. E., Woodruff, J. D., Donnelly, J. P., and Zhang, Z. H.: Atlantic hurricanes and climate over
464 the past 1500 years, *Nature*, 460, 1256–1260, 2009.
- 465 Mantua, N. J., Hare, S. R., Zhang, Y., Wallace, J. M., and Francis, R. C.: A Pacific interdecadal
466 climate oscillation with impacts on salmon production. *B. Amer. Meteorol. Soc.*, 78, 1069–1079,
467 1997.
- 468 Marelle, L., Myhre, G., Hodnebrog, Ø., Sillmann, J., and Samset, B. H.: The changing seasonality of
469 extreme daily precipitation, *Geophys. Res. Lett.*, 45, 11,352–11,360, 2018.
- 470 Mudelsee, M., Börngen, M., Tetzlaff, G., and Grünwald, U.: Extreme floods in central Europe over
471 the past 500 years: Role of cyclone pathway “Zugstrasse Vb”, *J. Geophys. Res.*, 109, D23101,
472 2004.
- 473 Pfister, C.: *Wetternachhersage: 500 Jahre Klimavariationen und Naturkatastrophen (1496–1995)*.
474 Haupt, Bern, 1999.
- 475 Pfister, C.: Die “Katastrophenlücke” des 20. Jahrhunderts und der Verlust traditionellen
476 Risikobewusstseins, *Gaia* 18, 239–246, 2009.
- 477 Pfister, C. and Brändli, D.: Rodungen im Gerbirge - Überschwemmungen im Vorland: Ein
478 Deutungsmuster macht Karriere. In: Sieferle, R. P., and Breuninger, H. (eds) *Natur-*
479 *Bilder. Wahrnehmungen von Natur und Umwelt in der Geschichte*, Campus Verlag, Frankfurt/Main
480 and New York, pp. 297–323, 1999.
- 481 Pfister, C.: *Das Klima der Schweiz von 1525 bis 1860 und seine Bedeutung in der Geschichte von*
482 *Bevölkerung und Landwirtschaft*. Paul Haupt, Bern, 184+163 pp., 1984.



- 483 Quinn, N. and Wilby, R. L.: Reconstructing multi-decadal variations in fluvial flood risk using
484 atmospheric circulation patterns. *J. Hydrol.*, 487, 109-121, 2013.
- 485 Rajczak, J., and Schär, C.: Projections of future precipitation extremes over Europe: A multimodel
486 assessment of climate simulations, *J. Geophys. Res.*, 122, 10,773–10,800, 2017.
- 487 Rohrer, M., Brönnimann, S., Martius, O., Raible, C. C., Wild, M., and Compo, G. P.: Representation
488 of cyclones, blocking anticyclones, and circulation types in multiple reanalyses and model
489 simulations, *J. Clim.*, 31, 3009–3031, 2018.
- 490 Rössler, O., and Brönnimann, S.: The effect of the Tambora eruption on Swiss flood generation in
491 1816/1817, *Sci. Tot. Env.*, 627, 1218-1227, 2018.
- 492 Schmocker-Fackel, P., and Naef, F.: Changes in flood frequencies in Switzerland since 1500, *Hydr.*
493 *Earth. Sys. Sci.*, 14, 1581–1594, 2010a.
- 494 Schmocker-Fackel, P., and Naef, F.: More frequent flooding? Changes in flood frequency in
495 Switzerland since 1850, *J. Hydrol.*, 381, 1–8, 2010b.
- 496 Schwander, M., Brönnimann, S., Delaygue, G., Rohrer, M., Auchmann, R., and Brugnara, Y.:
497 Reconstruction of Central European daily weather types back to 176., *Int. J. Climatol.*, 37, 30-44,
498 2017.
- 499 Stewart, M. M., Grosjean, M., Kuglitsch, F. G., Nussbaumer, S. U., and von Gunten, L.:
500 Reconstructions of late Holocene paleofloods and glacier length changes in the Upper Engadine,
501 Switzerland (ca. 1450 BC–AD 420), *Palaeogeogr. Palaeoclimatol. Palaeoecol.*, 311, 215–223, 2011.
- 502 Stucki, P. and Luterbacher, J.: Niederschlags-, Temperatur- und Abflussverhältnisse der letzten
503 Jahrhunderte, *Hydrologischer Atlas der Schweiz, Tafel 1.4 (HADES 1.4)*, 2010.
- 504 Stucki, P., Rickli, R., Brönnimann, S., Martius, O., Wanner, H., Grebner, D., and Luterbacher, J.:
505 Weather patterns and hydro-climatological precursors of extreme floods in Switzerland since 1868,
506 *Meteorol. Z.*, 21, 531-550, 2012.
- 507 Sturm, K., Glaser, R., Jacobeit, J., Deutsch, M., Brazdil, R., Pfister, C., Luterbacher, J., and Wanner,
508 H.: Hochwasser in Mitteleuropa seit 1500 und ihre Beziehung zur atmosphärischen Zirkulation,
509 *Peterm. Geogr. Mitt.*, 145 (6), 14-23, 2001.
- 510 Summermatter, S.: Die Überschwemmungen von 1868 in der Schweiz, Verlag Traugott Baulz, 352.
511 pp., 2005.
- 512 Sutton, R. T. and Hodson, D. L.: Atlantic Ocean forcing of North American and European summer
513 climate, *Science*, 309, 115-118, 2005.
- 514 Trenberth, K. E., and Shea D. J.: Atlantic hurricanes and natural variability in 2005, *Geophys. Res.*
515 *Lett.*, 33, L12704, 2006.
- 516 Wanner, H., Beck, C., Brazdil, R., Casty, C., Deutsch, M., Glaser, R., Jacobeit, J., Luterbacher, J.,
517 Pfister, C., Pohl, S., Sturm, K., Werner, P. C., and Xoplaki, E.: Dynamic and socioeconomic
518 aspects of historical floods in Central Europe, *Erdkunde*, 58, 1-16, 2004.
- 519 Wetter, O., Pfister, C., Weingartner, R., Luterbacher, J., Reist, T., and Trösch, J.: The largest floods in
520 the High Rhine basin since 1268 assessed from documentary and instrumental evidence, *Hydrol.*
521 *Sci. J.*, 56, 733–758, 2011.
- 522 Weusthoff, T.: Weather Type Classification at MeteoSwiss: Introduction of New Automatic
523 Classification Schemes. Bundesamt für Meteorologie und Klimatologie, MeteoSchweiz, 2011.



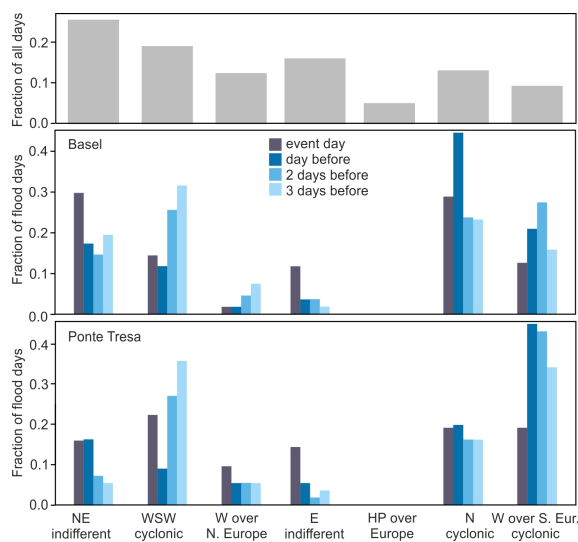
524 **Figures**



525

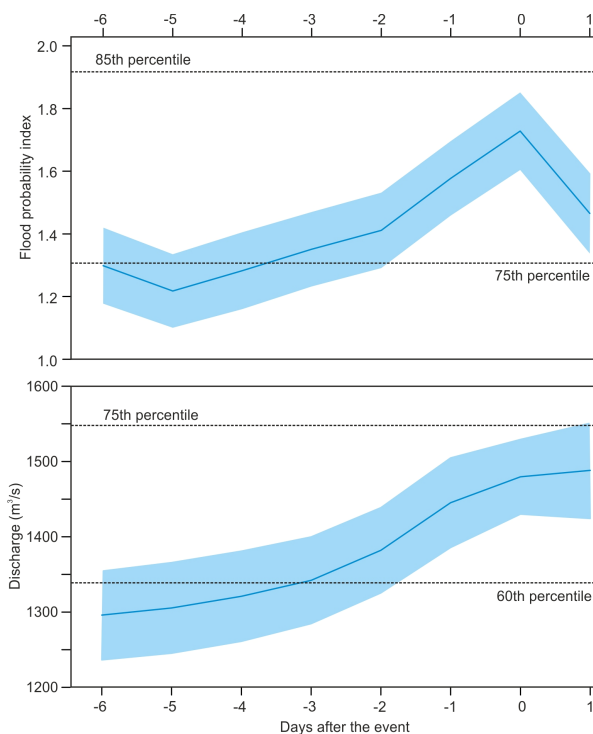
526 **Fig. 1.** Topographic map of the central Alps showing the catchments and locations mentioned in the
 527 text, the catchments of the Rhine in Basel (orange), Lake Constance (dark blue), Lago Maggiore (light
 528 blue) and Ponte Tresa (red). The rectangle boxes indicate the areas chosen for averaging precipitation
 529 in the HISTALP data.

530



531

532 **Fig. 2.** Frequency of CAP7 weather types in the warm season (top). Fraction of flood days occurring
 533 during a specific weather types for Basel (middle) and Ponte Tresa (bottom) as well as corresponding
 534 series for days 1 to 3 prior to the discharge peak. The figure is based on data from 1901-2000

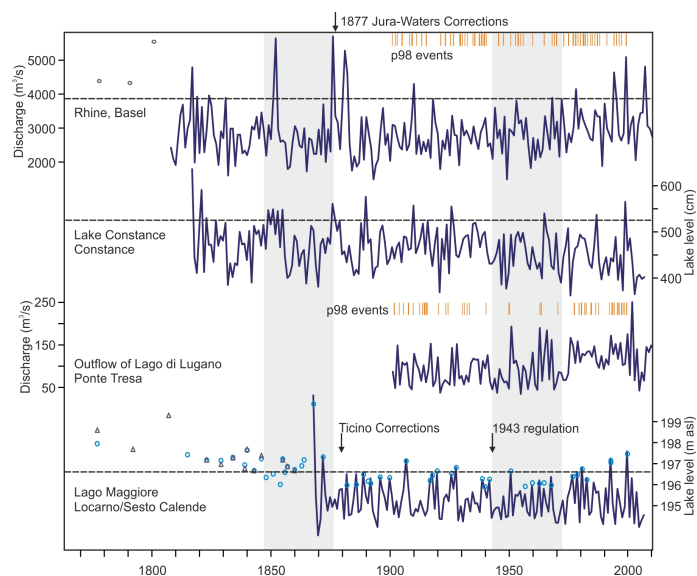


535

536 **Fig. 3.** Composites of the daily flood probability index for peak-over threshold discharge events in
537 Basel (top), and composites of discharge in Basel for peak-over threshold FPI events (bottom) for 6
538 days preceding to 1 day following event day (day 0). Shading indicates the 95% confidence interval of
539 the mean value. Selected percentiles are indicated as dashed lines.



540

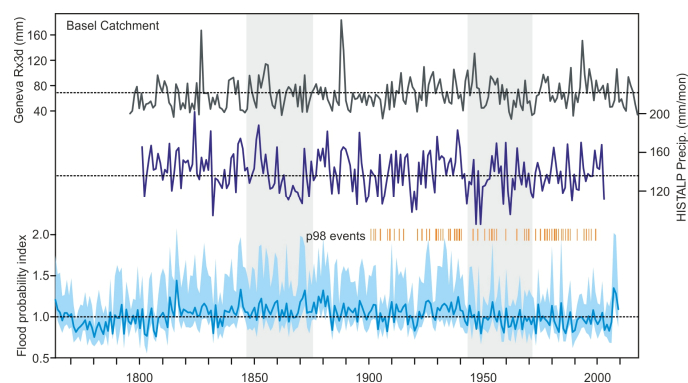


541

542 **Fig. 4.** Time series of annual maxima of discharge or lake level in four catchments. Symbols denote
543 reconstructed floods based on historical sources (circles for Rhine, Basel, from Wetter et al. 2011,
544 Triangles for Lago Maggiore, Locarno, from Stucki and Luterbacher, 2010, light blue circles for Lago
545 Maggiore refer to floods at Sesto Calende according to Di Bella, 2005, from reconstruction prior to
546 1829 and measurements afterwards, adjusted to Locarno by adding the average difference between the
547 two during floods after 1868, i.e., 0.49 m). Arrows indicate major river corrections. Orange bars
548 indicate the peak-over threshold events in the 1901-2000 period that were used to calibrate the FPI.
549 Grey shading denotes the flood-rich period in the 19th and flood-poor period in the 20th century.
550 Dashed lines indicate the 95th percentile from 1901-2000.



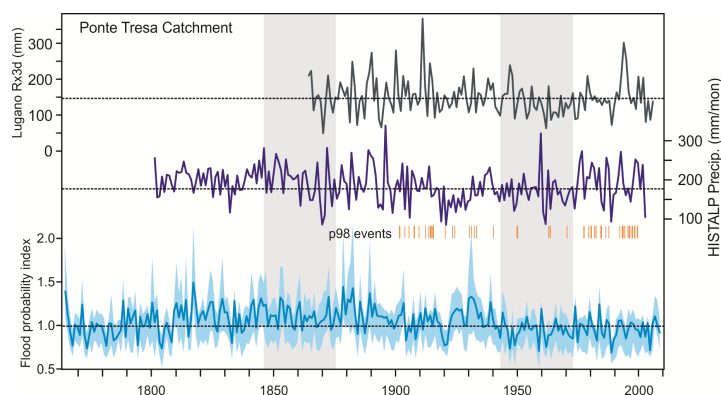
551



552

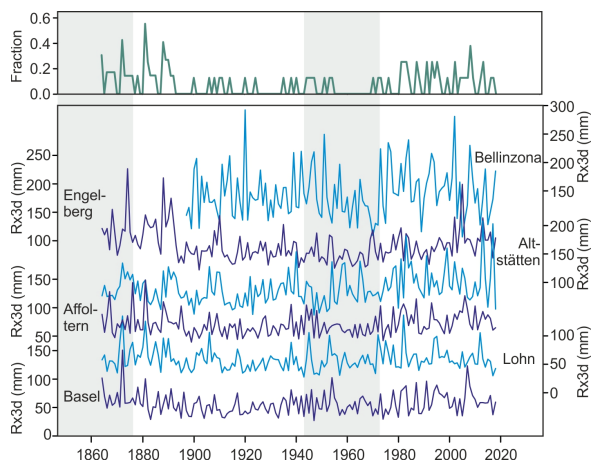
553 **Fig. 5.** Warm season Rx3d from the station Geneva (top), warm season mean precipitation in
554 HISTALP for the Rhine catchment (middle) and flood probability index for Basel (bottom, solid
555 indicates the warm season mean, shading indicates the median and 75th percentile, respectively).
556 Dashed lines indicate the 1901-2000 average. Also shown are the peak-over threshold events (p98) of
557 Basel discharge that were used for calibration.

558



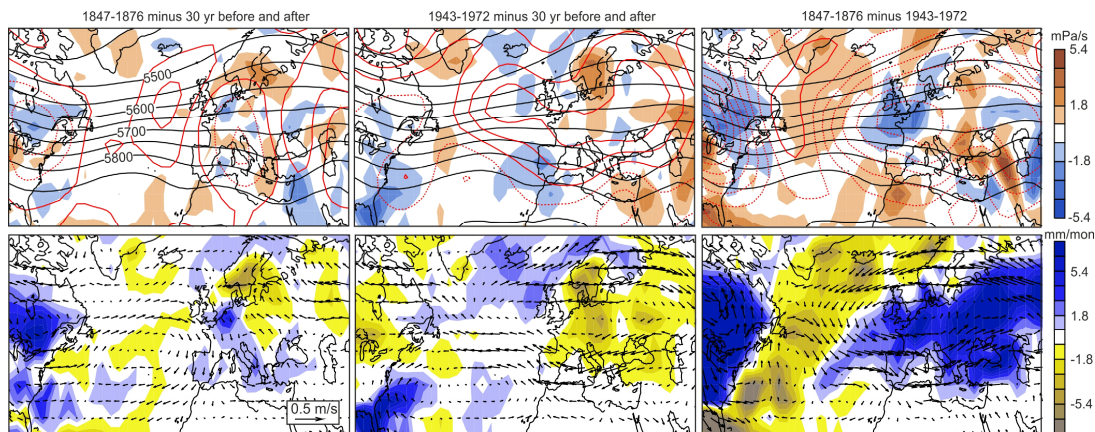
559

560 **Fig. 6.** Warm season Rx3d from the station Lugano (top), warm season mean precipitation in
561 HISTALP for the Ponte Tresa catchment (middle) and flood probability index for Ponte Tresa
562 (bottom, solid indicates the warm season mean, shading indicates the median and 75th percentile,
563 respectively). Dashed lines indicate the 1901-2000 average. Also shown are the peak-over threshold
564 events (p98) of Ponte Tresa discharge that were used for calibration.



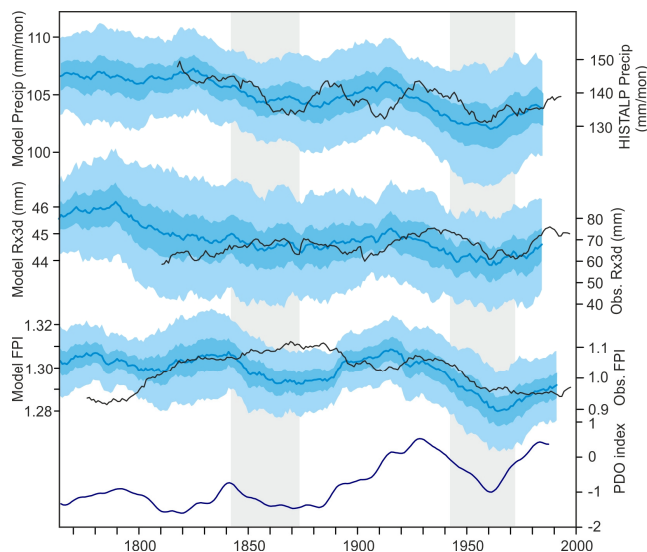
565

566 **Fig. 7.** Series of Rx3day for six further stations with long precipitation series (see Fig. 1 for locations).
 567 The top line shows the fraction of these six series plus those of Lugano and Geneva shown in Figs. 5
 568 and 6, exceeding their 95th percentile (based on 1901-2000) in any given year.



569

570 **Fig. 8.** Anomalies of (top) 500 hPa GPH (red contours, 2 gpm spacing symmetric around zero,
 571 negative contours are dashed, black lines indicate the reference period average) and vertical velocity
 572 (colours, lifting is blue) and (bottom) 850 hPa wind and precipitation. Shown are anomalies for the
 573 1847-1876 period (left) and the 1943-1972 period (middle) with respect to the 30 yrs before and after
 574 as well as (right) the difference between the two periods.



575

576 **Fig. 9.** CCC400 (left scales) warm season average precipitation (top, note that this series was
577 detrended based on the corrected member), Rx3day in the warm season at the grid point north of the
578 Alps (second from top) and flood probability index based on weather types in CCC400 (third from
579 top). The lowest line shows the PDO index in the model simulations. The solid blue lines show the
580 ensemble mean of the series smoothed with a 31-yr moving average. Light and dark shadings indicate
581 the ensemble standard deviation and the 95% confidence interval of the ensemble mean, respectively.
582 Black lines (right scales) show the corresponding observation-based series. Note the different scales.

583